View metadata, citation and similar papers at core.ac.uk
brought to you by CORE
provided by IR@NPL

Int. J. Electrochem. Sci., 9 **(2014)** 955 - 974

International Journal of
ELECTROCHEMICAL
SCIENCE
www.electrochemsci.org

Structural, Electronic and Optical Properties in Earth-Abundant Photovoltaic Absorber of Cu_2ZnSnS_4 and $Cu_2ZnSnSe_4$ from DFT calculations

A. H. Reshak[1,2,*], *K. Nouneh*[3], *I.V. Kityk*[4,7], *Jiri Bila*[5], *S. Auluck*[6], *H. Kamarudin*[2], *Z. Sekkat*[3,8]

[1] New Technologies - Research Center, University of West Bohemia, Univerzitni 8, Pilsen 306 14, Czech Republic
[2] Center of Excellence Geopolymer and Green Technology, School of Material Engineering, University Malaysia Perlis, 01007 Kangar, Perlis, Malaysia
[3]Moroccan Foundation for Advanced Science, Innovation and Research (MAScIR), Optics & Photonics, ENSET, Av. Armée Royale 10100, Rabat, Morocco
[4]Electrical Engineering Department, Czestochowa University of Technology, Armii Krajowej 17, Czestochowa, Poland
[5]Department of Instrumentation and Control Engineering, Faculty of Mechanical Engineering, CTU in Prague, Technicka 4, 166 07 Prague 6, Czech Republic
[6]Council of Scientific and Industrial Research - National Physical Laboratory Dr. K S Krishnan Marg, New Delhi 110012, India
[7]Eastern European University, Physical Department, Al Voli 6, Lutsk, Ukraine
[8]University Mohamed V-Agdal, Faculty of Sciences, Rabat, Morocco
[*]E-mail: maalidph@yahoo.co.uk

Received: 24 August 2013 / *Accepted:* 7 October 2013 / *Published:* 1 December 2013

DFT analyses of band structure dispersion and of contribution of different anionic sub-groups to the studied electronic structure together with the anisotropy of optical functions were performed for the two promising solar cell crystals Cu_2ZnSnS_4 and $Cu_2ZnSnSe_4$. We have applied the state-of-the-art full potential linear augmented plane wave (FPLAPW) method in a scalar relativistic version. Exchange and correlation potential were introduced within a framework of the local density approximation (LDA) and gradient approximation (GGA). We show that Cu_2ZnSnS_4 as well as $Cu_2ZnSnSe_4$ crystals possess a direct energy band gap situated around the center of the BZ. Careful analysis of the total density of states together with the partial contribution of the particular orbital were performed for evaluations of contribution of corresponding bonds to the origin of the chemical bonds. Role of replacing of S by Se is analyzed in the details for the electronic density of states with respect to the nature of chemical bonds. The principal analysis is performed for the dispersion of the optical constants. The influence of the different chemical bonds into the dispersion of the optical functions is analyzed in order to optimize the optical features with respect to the requirements of the solar cell elements.

Keywords: CZTS Kesterites;Cu_2ZnSnS_4; optical functions; DFT band structure calculations

1. INTRODUCTION

To decrease the consumption of fossil fuels, energy sources like solar energy must be advanced. Solar cells are an alluring energy source, as they do not cause any detrimental emissions. In the many solar cell materials as a rule the Si-based solar cell is mostly used. Ideally, the absorber material of an efficient terrestrial solar cell should be a direct bandgap semiconductor with a bandgap of 1.5 eV with a high solar optical absorption (~10^5/cm) high quantum efficiency of excited carriers, long diffusion length, low recombination velocity, and should be able to form a good electronic junction (homo/hetero/Schottky) with suitably compatible materials. With high optical absorption, the optimum thickness of an absorber in a solar cell is of the order of the inverse of the optical absorption coefficient and thus it must be a thin-film. The I–III–VI2 ternary compounds like CIS and CIGS etc, and their alloys CuInxGa1−xSe2 (CIGSe) are considered to be suitable absorber materials in low-cost and high-efficiency thin-film solar-cell technologies. Recently, the Cu2ZnSnS4 (CZTS) absorber has drawn an increasing amount of attention within thin-film solar cell technology owing to its optimal single-junction band gap (~1.5 eV) and high absorption coefficient (~10^5 cm−1) [1–3], in which the expensive group-III elements (i.e., In and Ga) are substituted by group-II-IV elements (e.g. Zn plus Sn), thereby forming the I2–II–IV–VI4 quaternary compound Cu2ZnSnSe4 (CZTSe) and its sulfide counterpart Cu2ZnSnS4 (CZTS). The band-gap energy Eg of the CIGSe alloy can be tuned from 1.04 to 1.68 eV and the gap energies of CZTS and CZTSe are around 1.0–1.5 eV, which is suitable for photovoltaic applications. Moreover, knowledge of the optical properties, such as the dielectric function and the optical absorption coefficient, is required to analyze optical measurements as well as to optimize the solar cell devices.

Recently, a solar-cell conversion efficiency of 10.1% was reported [4] for the mixed sulfide–selenide CZTSSe absorber made by hydrazine-based solution processing. For the nominal intrinsic CZTS, the highest efficiency has reached 8.4% [5]. To obtain this high efficiency, the Cu-poor and Zn-rich condition in CZTS is currently necessary.

The CZTS thin film exists in two types of crystal structures kesterite and stannite [6]. Schorr [7,8] has established that both crystal structures are tetragonal, except the difference between them is the site position of their Cu and Zn atoms. The crystal structure of isomorphic crystals is important infor calculation of their band structure. [9]. Their electronic properties and crystal structures are analogous to those of the parent CIGS, while their constituent elements are naturally copious and nontoxic. According to the Shockley–Queisser limit the $Cu_2ZnSnS_xSe_{1-x}$ have gaps and usually are used as absorbers in thin film solar cells favoring growing energy conversion efficiency [10,11]. Though, the understanding of the properties of Cu_2ZnSnS_4 and $Cu_2ZnSnSe_4$ for the different phases is still rather cursory, recent studies have reported their structural,[12-14] electronic [12,13,15] and defect properties.[16,17]. Nozaki et al. [18] experimentally determined the crystal structure of Cu_2ZnSnS_4 thin films fabricated by vapor-phase sulfurization using X-ray anomalous dispersion. He and Shen [19] perform first principles study of elastic and thermo-physical properties of kesterite type

Cu_2ZnSnS_4 , using VASP code. They found that the calculated lattice constants are in good agreement with the experimental data. Persson [20] studied the electronic and the optical properties of Cu_2ZnSnS_4 and $Cu_2ZnSnSe_4$ using FPLAPW-LDA. Chen et al. [21] have used the VASP code to study the structural and electronic properties of Cu_2ZnSnS_4 and $Cu_2ZnSnSe_4$.

From above it is clear that there is no comprehensive research work neither experimental nor theoretical one were done for these compounds Cu_2ZnSnS_4 and $Cu_2ZnSnSe_4$. Thus we thought it would be worthwhile to perform such comprehensive investigation for such kind of important materials. Therefore we have calculated the electronic band structure, density of states, electronic charge density and the optical properties of Cu_2ZnSnS_4 and $Cu_2ZnSnSe_4$ using the full potential method.

The main goal of the present work is to perform DFT analysis of the band structure dispersion of Cu_2ZnSnS_4 and $Cu_2ZnSnSe_4$ and also to perform analysis of contribution of different anionic sub-groups to the studied electronic structure. Following these calculations the analysis of the electronic density of states and the modeling of the corresponding optical constants dispersions will be calculated. Section 2 presents principal crystallochemistry analysis and applied calculation technique. Section 3 is devoted to presentation of the band structure calculations, electronic density of states, and the dispersion of principal optical functions.

2. CRYSTAL STRUCTURES AND COMPUTATIONAL DETAILS

Table 1. Crystallographic lattice parameters for the compounds Cu_2ZnSnS_4 [15] and $Cu_2ZnSnSe_4$ [16]

	Cu_2ZnSnS_4	$Cu_2ZnSnSe_4$
SG	$I\bar{4}2m$ (no. 121)	
a (Å)	5.434(1)	5.6882(2)
c (Å)	10.856(1)	11.3378(9)
4*d* (0 ½ ¼)	0.5Cu+0.5Zn	Cu
2*a* (0 0 0)	Cu	Zn
2*b* (0 0 ½)	Sn	Sn
8*i* (*x x z*)	S (*x*=0.75617(8), *z*= 0.87208(5)	Se (*x*=0.2587(2), *z*=0.3714(2))

Crystallographic parameters for the chalcogenide Cu_2ZnSnS_4 [22] and $Cu_2ZnSnSe_4$ [23] are given in Table 1. The second coordination number of chalcogen atoms in the compound Cu_2ZnSnS_4 and $Cu_2ZnSnSe_4$ were presented in Fig. 1. Generally consideration of the second anionic group is very efficient way to analyze the chalcogenide structures [24]. One can see cubooctahedra containing chalcogen atoms and cationic atoms are situated opposite triangle faces which corresponds to their tetrahedral coordination. Second coordination is formed by chalcogen atoms and define principal inter-atomic distances within the anionic group of $Cu_2ZnSnS(Se)_4$ system. Inter-atomic distances chalcogen-chalcogen are slightly greater with respect to the sum of their atomic radiuses and the bond lengths

anion-cation are shortened (r_{Se}^{-2} = 1.91, r_S^{-2} = 1.82, r_{Cu}^{+1} = 0.96, r_{Zn}^{+2} = 0.83, r_{Sn}^{+4} = 0.71 [25]). This one confirms prevailingly ionic cationic-anionic origin of the chemical bonds.

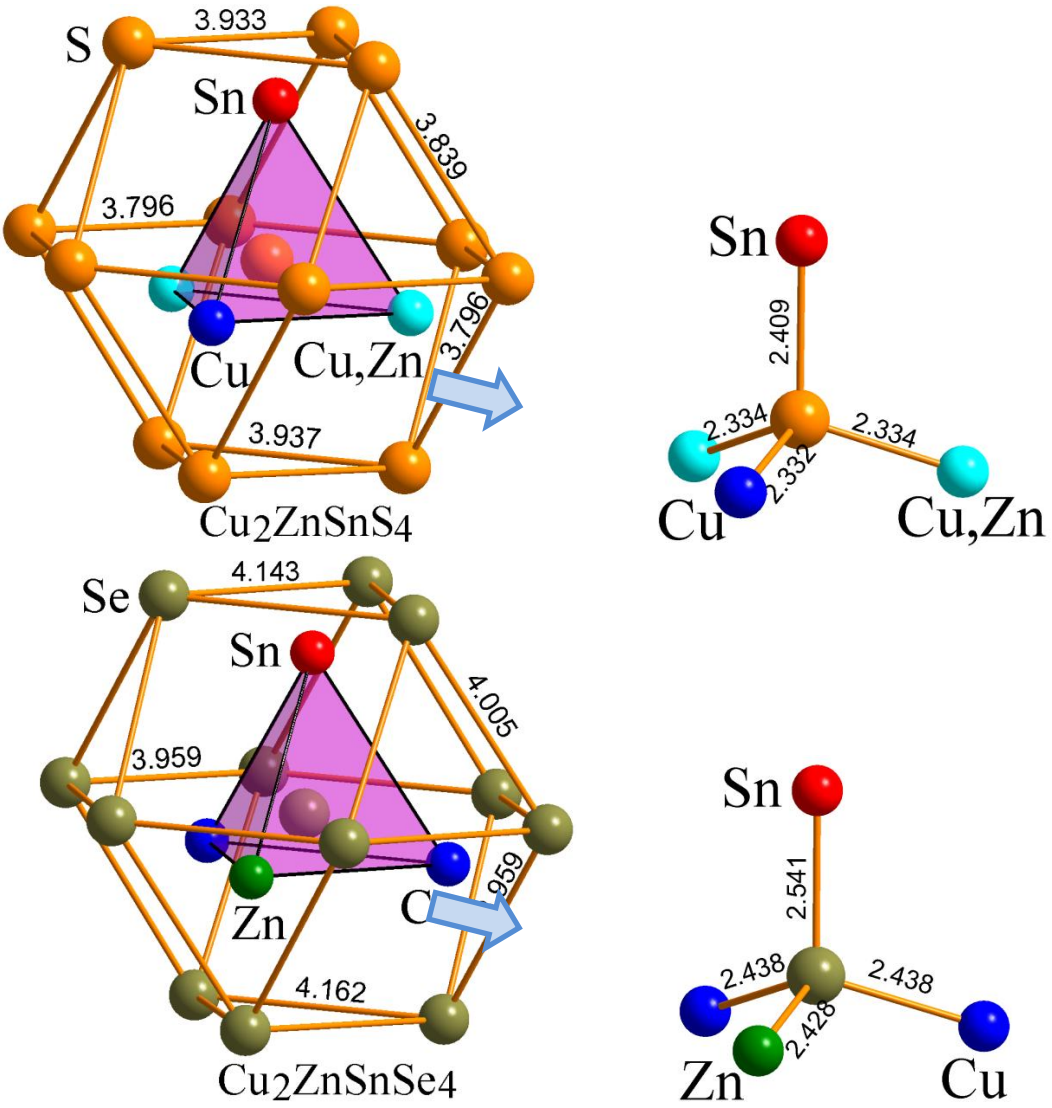

Figure 1. Second coordination surrounding of chalcogen atoms and inter-atomic distances within the anionic group of $Cu_2ZnSnS(Se)_4$ system. Inter-atomic distances chalcogen-chalcogen are slightly higher with respect the sum of their atomic radiuses and the bond lengths anion-cation are shortened (r_{Se}^{-2} = 1.91, r_S^{-2} = 1.82, r_{Cu}^{+1} = 0.96, r_{Zn}^{+2} = 0.83, r_{Sn}^{+4} = 0.71 [17]). This one confirm prevailingly ionic cationic-anionic origin of the chemical bonds

We have applied the state-of-the-art full potential linear augmented plane wave (FPLAPW) method in a scalar relativistic version as embodied in the WIEN2k code [26]. This is an implementation of the DFT with different possible approximations for the exchange-correlation (XC) potential. Exchange and correlation potential were introduced within a framework of the local density approximation (LDA) [27] and gradient approximation (GGA) [28], which is build applying exchange-correlation energy optimization to evaluate the minimum of total energy. We also have used Engel-

Vosko generalized gradient approximation (EV-GGA) [29] and the modified Becke-Johnson potential (mBJ) [30], which serve for optimization of the corresponding potential for electronic band structure calculations. These methods are very efficient for studies of the semiconducting materials with relatively narrow band energy gaps. The FP-LAPW method is more efficient for the materials possessing different degree of wave functions localization. That means for the crystals where exists a coexistence of delocalized covalence and high localized d-p chemical bonds use of the mentioned methods may be very powerful [31,32]. The Kohn-Sham equations were solved using a basis of linear APW's. The potential and charge density distributions intra the muffin-tin (MT) spheres are expanded in spherical harmonics with orbital number $l_{max}=8$ and nonspherical components up to $l_{max}=6$. In the interstitial space the potential and the charge density were represented by Fourier series. The chosen MT sphere radii of Cu_2ZnSnS_4 were 2.29, 2.35, 2.31, 2.03 a.u. for Cu, Zn, Sn, and S, respectively and for $Cu_2ZnSnSe_4$ are 2.38, 2.46, 2.44 and 2.11 a.u., for Cu, Zn, Sn and Se, respectively. The structure of the chalcogenide Cu_2ZnSnS_4 and $Cu_2ZnSnSe_4$ was optimized by minimization of forces acting on the atoms to get optimized with respect to the mixed relaxed geometry. Self-consistency was achieved just at 300 $\vec{k}$ points in the irreducible Brillouin zone (IBZ). However for the optical functions it was necessary to use more number of the points within the BZ (about 500 $\vec{k}$ points in the IBZ).

3. RESULTS AND DISCUSSION

3.1 Band structure parameters and density of state

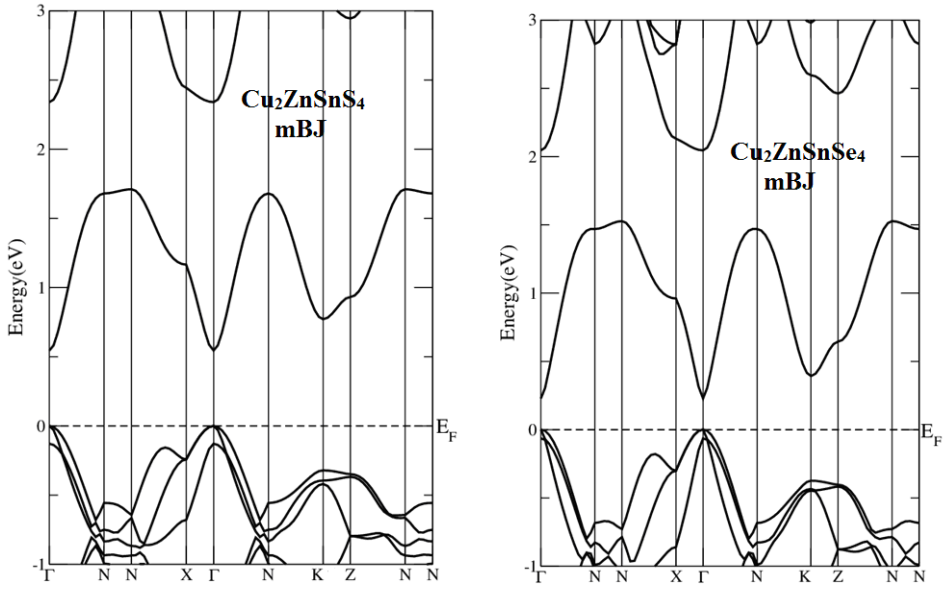

Figure 2. Calculated band structure using mBJ.

The study of band structure for the photovoltaic material and particularly for the crystal presents very important task. It allow to evaluate the spectral distribution of the absorption, charge

density distribution, their mobility etc. The evaluated optical features may serve as a basis for the further optimization of the electronic properties in the desired direction.

The calculated band structure dispersion in ***k***-space along high symmetry directions in the BZ, the total and partial density of states are presented in Fig. 2 and 3. Following Fig.2, one can see that both Cu_2ZnSnS_4 as well as $Cu_2ZnSnSe_4$ crystals possess a direct energy band gap situated around the center of the BZ.

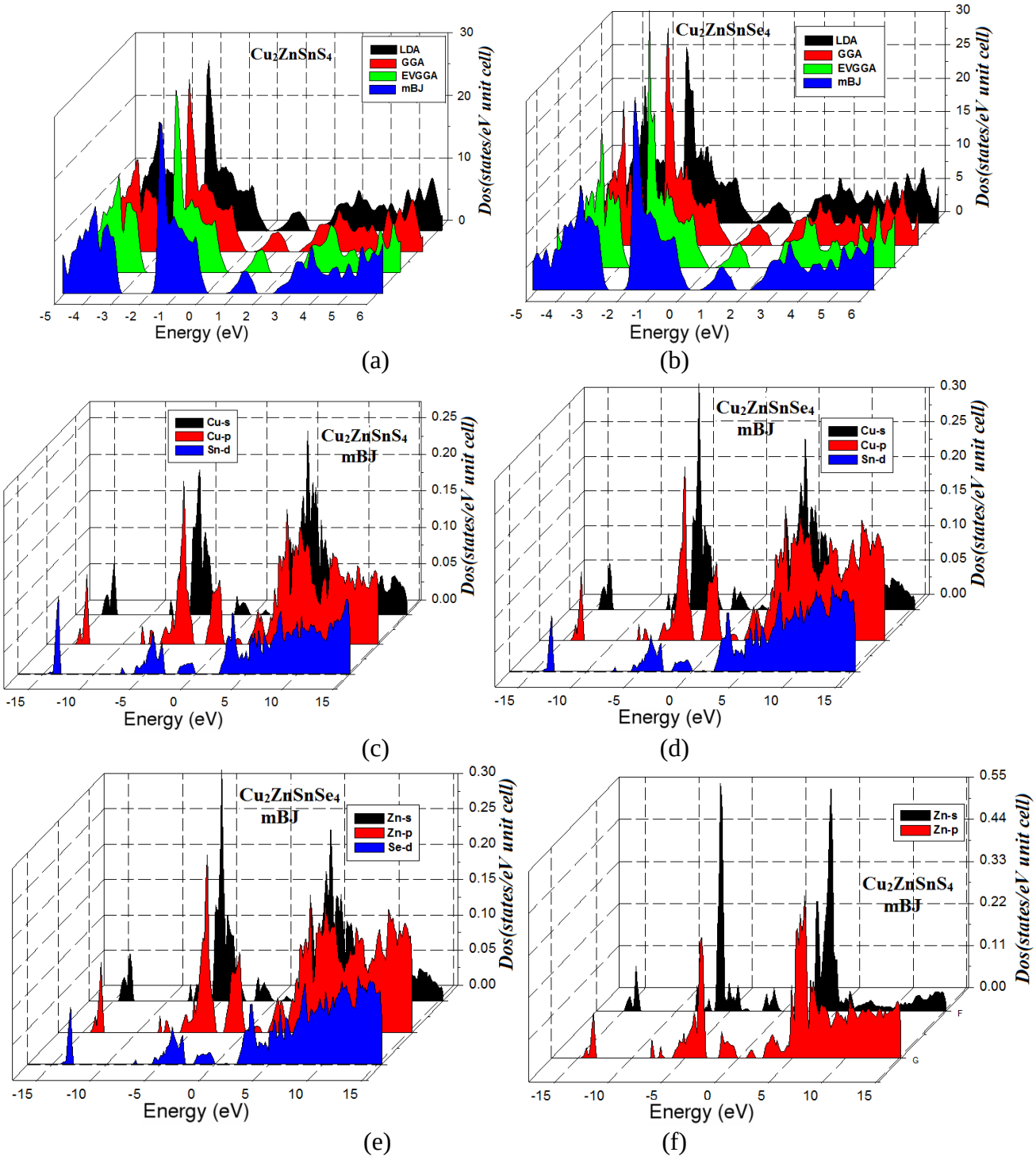

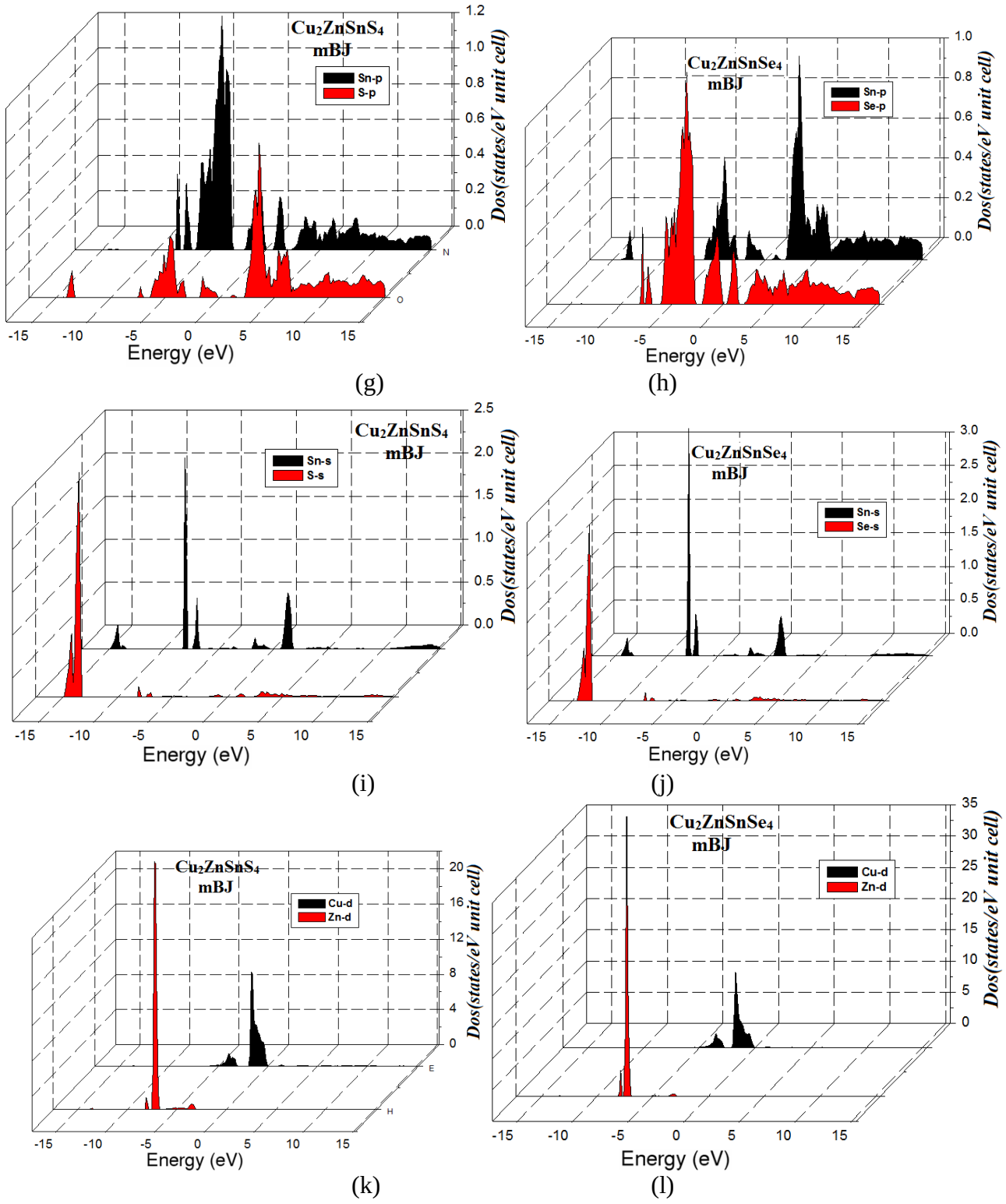

Figure 3. Calculated total and partial densities of states (States/eV unit cell) using LDA, GGA, EVGGA and mBJ.

The calculated values of the band gaps are 0.54 eV and 0.22 eV for Cu_2ZnSnS_4 and $Cu_2ZnSnSe_4$, respectively. It is principal that the energy gap is reduced with replacing S to Se, this

reduction is attributed to the fact that Se atoms have bigger radius (1.17 Å) than S (1.17 Å) and the atomic terms of pSe lie higher in energy the atomic terms of pS.

These terms are responsible for the formation of the VB . In the periodic table when we move down in group there is an increase in the bond length of the compounds (see Fig. 1) resulting in decrease of the band gap. In other hand, the electronegativity value of S is 2.58 and 2.55 for Se, respectively. Thus, when S is replaced by Se it leads to an increase of the bond length. Oppositely increase in the bond length results in a decrease in the band gap. Following Fig. 2, it is clear that the conduction band of $Cu_2ZnSnSe_4$ is shifted towards Fermi level with respect to Cu_2ZnSnS_4.

The total density of states (TDOS) for $Cu_2ZnSnSe_4$ and Cu_2ZnSnS_4 were calculated using four type of XC screening potentials. Our calculations confirm the substantial influence of different kinds of XC potentials on the electronic structure features. We should remind that for the all full potential methods the potential and charge densities are expanded into lattice harmonics inside each atomic sphere and as a Fourier series in the interstitial region. As a remarkable finding, mBJ [42-46] form gives energy band gap larger then LDA, GGA, and EVGGA approaches. Thus we will demonstrate only the results obtained by mBJ.

For these crystals the unit cell contains four atoms. In order to understand the contribution of each orbital in these atoms we investigate the angular momentum decomposition of the atoms projected density of states (PDOS) as illustrated in the Fig. 3 c-l. The PDOS helps to identify the angular momentum character of the various structures; the lowest structure extended from -15.0 eV up to -5.0 eV originated mainly from Sn-s, Se/S-s, Se/S-p, Sn-p, Zn-d states with small admixture of Zn-s/p, Se-d, Cu-s/p and Sn-d states. All these orbitals are spatially delocalized. Next energy fragment - from -5.0 eV till Fermi level (E_F) originates from more localized Cu-d, and delocalized Se/s-p, Sn-p states with small contribution from Sn-s/d, Zn-s/p, Se-d, Cu-s/p states. Finally the structure from the conduction band minimum and above presents an admixture of Cu-s/p, Sn-p/d, Zn-s/p, Se-s/p/d and S-p states. One can see a strong hybridization between Cu-p, Zn-d and Sn-d states and also some overlap between Se-s and Sn-s states, at around -13.5 eV. At -8.0 eV there is relatively strong hybridization between Se-p and Sn-s, Sn-s and S-p states as well as between Zn-s/p and Cu-s/p states. At the energies lying between -3.5 eV to -1.0 eV there is a strong hybridization between Se-d and Se-p. Between 1.0 eV to 4.0 eV there occurs also a strong hybridization between Sn-s and Se/S-p states and also between Sn-d and Cu-s states.

3.2. Electron charge density

Now we will analyze and express the electronic charge density of $Cu_2ZnSnSe_4$ and Cu_2ZnSnS_4, to obtain a deeper insight into the electronic structure, we displayed the electronic charge density contour in the (203) crystallographic plane as shown in Fig. 4a. The contour plot shows partial ionic and strong covalent bonding between Cu-S/Se and Zn-S/Se atoms depending on Pauling electro-negativity difference of Cu (1.90), Zn (165) Sn (1.96), and S/Se (2.58/2.55) atoms. From these contour plots one can see that the majority of Cu, Zn, and Sn electronic charge is transferred to S/Se atom. This can be seen easily by the color charge density scale where blue color (+1.0000) corresponds to the

maximum charge accumulating site. The charge density along Cu-S/Se, Zn-S/Se bonds is pronounced. It is clear that when we replace S by Se the charge density decreases. As it is clear from Fig. 4a, that the charge density around the S is greater than the Se. the bond length between Zn and Se decrease as we replace S by Se which is not shown in Fig.4a. In additional we have plotted the electronic charge density contour in the (100) crystallographic plane as shown in Fig.4b. In this plane only three atoms namely Zn, Cu and Sn, from both of $Cu_2ZnSnSe_4$ and Cu_2ZnSnS_4 are contributed.

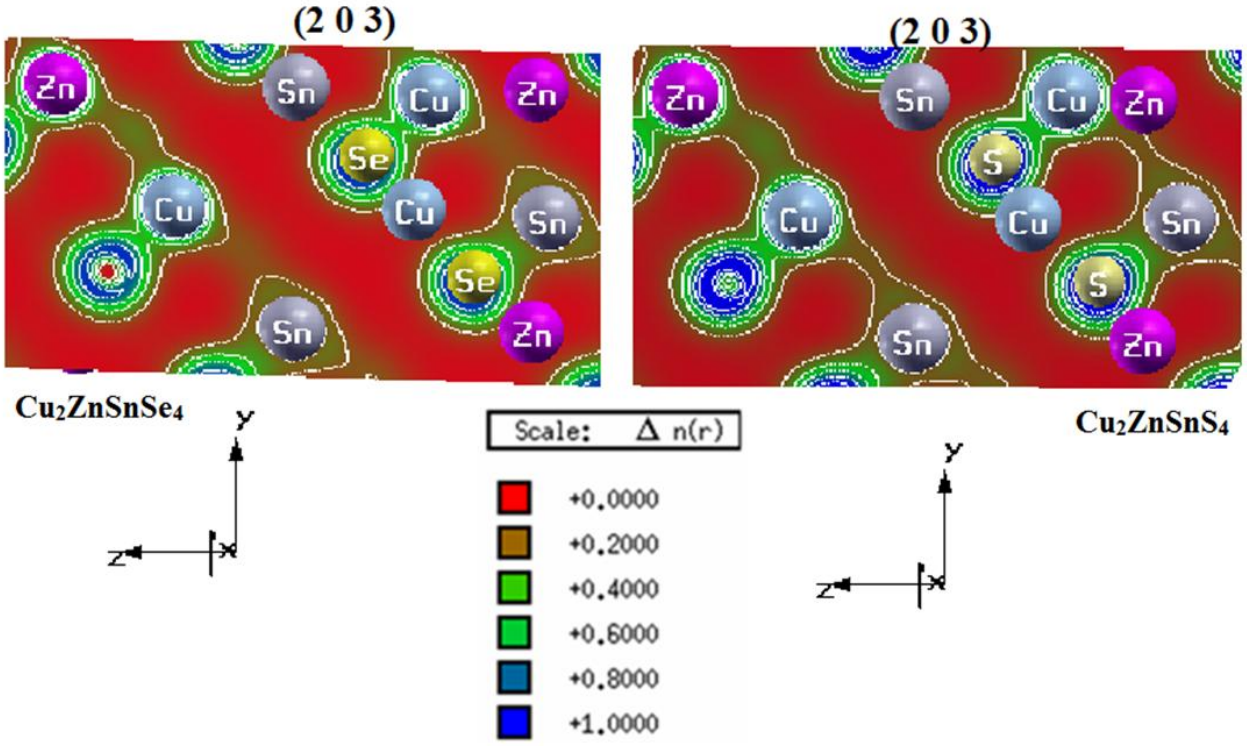

(a)

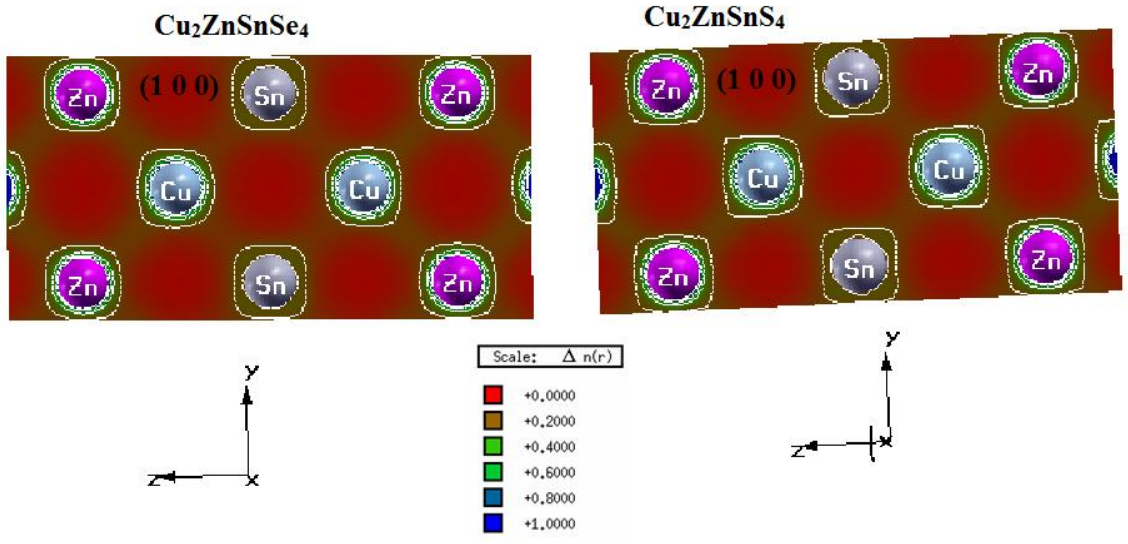

(b)

Figure 4. Electronic Charge density

3.3. Dispersion of optical permittivity

The dispersion of optical permittivity was evaluated from the energy eigenvalues and electron wave functions . Since the crystals are crystallized in tetragonal structure, following this symmetry one can observe only two non-zero components of second order dielectric tensor, i.e. $\varepsilon^{xx}(\omega)$ and $\varepsilon^{zz}(\omega)$. The two tensor components of the imaginary part of dielectric function (permittivity) completely define the principal linear optical dispersions responsible for absorption , refractive indices and reflection spectra. It should be emphasized that the contribution of the different BZ points will be different due to the van Howe singularities [33]. The dispersion of imaginary part can be calculated using the expression give in Ref. 34:

$$\varepsilon_2^{ij} = \frac{4\pi^2 e^2}{Vm^2\omega^2} \times \sum_{nn'\sigma} \left\langle kn\sigma \middle| p_i \middle| kn'\sigma \right\rangle \left\langle kn'\sigma \middle| p_j \middle| kn\sigma \right\rangle \times f_{kn}(1 - f_{kn'}) \delta(E_{kn'} - E_{kn} - \hbar\omega)$$

In this expression the indices *m* and *e* mean mass and charge of electron and ω represent the varying optical frequency, *V* stand for volume of the unit cell, in bracket notation *p* represent the momentum operator, $|kn\sigma\rangle$ describes the crystal wave function with crystal momentum *k* and σ spin which correspond to the eigenvalue E_{kn}. The Fermi occupation distribution function corresponds to f_{kn} which makes sure the counting of transition from occupied to unoccupied state and the term $\delta(E_{kn'} - E_{kn} - \hbar\omega)$ shows the condition for conservation of total energy. The phonons have negligible contribution to $\varepsilon_2(\omega)$, however their mainly define the broadening of the spectral lines [35], which may be fitted following the experimental data. Therefore we ignore the phonons contribution involved in the indirect inter-band transition introducing some experimentally obtained spectral half-width and only considering principal direct band transition between occupied VB and unoccupied CB states with the corresponding dipole matrix transitions moments. The spectral peaks in the optical response are caused by the allowed electric-dipole transitions between the VB and CB and here main contributions give the mentioned van Howe singularities. To identify these structures we analyze magnitudes of corresponding optical matrix elements.

It is well know that the DFT calculations usually underestimate the energy gaps with respect to the experimentally obtained gaps. Thus we have applied the scissors correction to the optical properties in order to fit the value of the calculated energy gap exactly to the measured one. This procedure was successively used by several workers for different organic and inorganic compounds [36]. The scissors correction is the difference between the calculated and measured energy gaps. After applying the scissors correction there occurs a significant effect on the magnitude, peaks positions and the structure of principal optical functions for the materials studied. This could arise from differences in the band structures and wave-functions.

The dispersion spectra of $\varepsilon_2(\omega)$ as illustrated in Figs. 5a and b, possess the threshold energy (first critical point) of the dielectric function occurring at 1.6 eV for Cu_2ZnSnS_4 and 1.44 eV for $Cu_2ZnSnSe_4$ crystals. The main structure of $\varepsilon_2^{xx}(\omega)$ and $\varepsilon_2^{zz}(\omega)$ is extended between the thresholds and 14.0 eV. One can see that the spectral structure for $\varepsilon_2^{xx}(\omega)$ and $\varepsilon_2^{zz}(\omega)$ for the both crystals are similar except some minor spectral deviations. Moreover, the whole structure is shifted towards lower energies

when we replace S by Se due to the band gap decreases and the changes in the band energy dispersions.

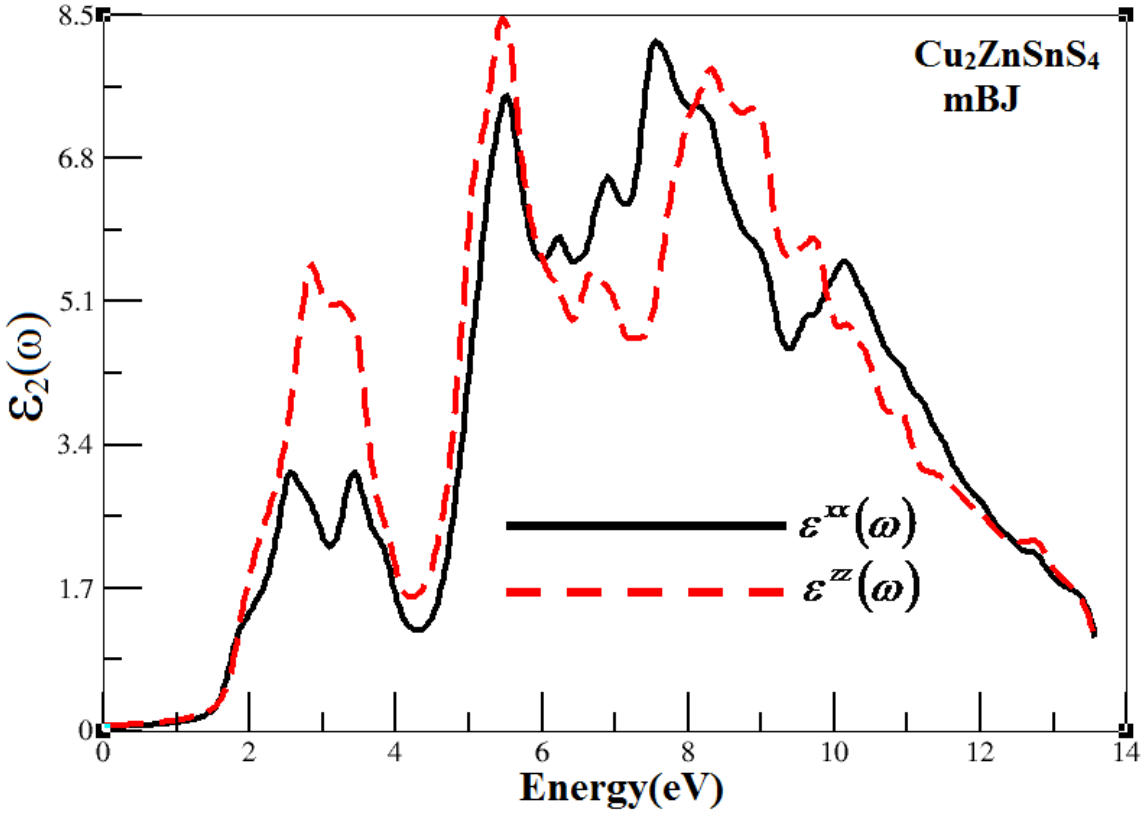

(a)

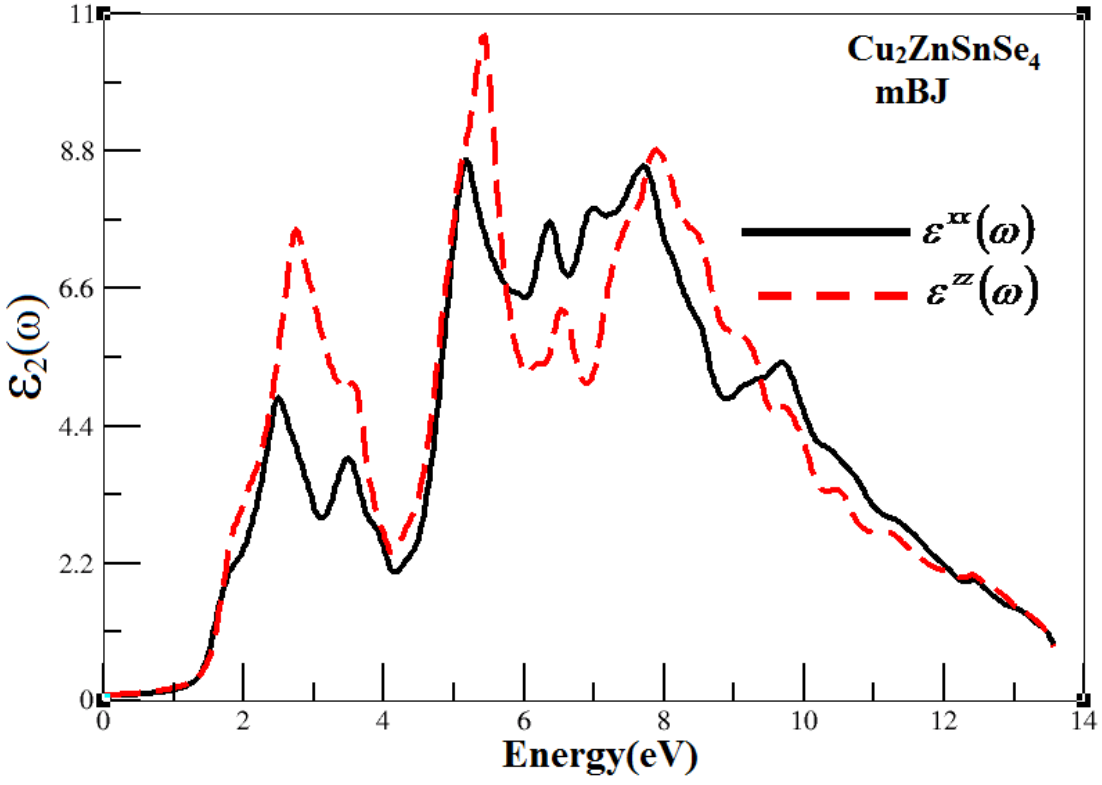

(b)

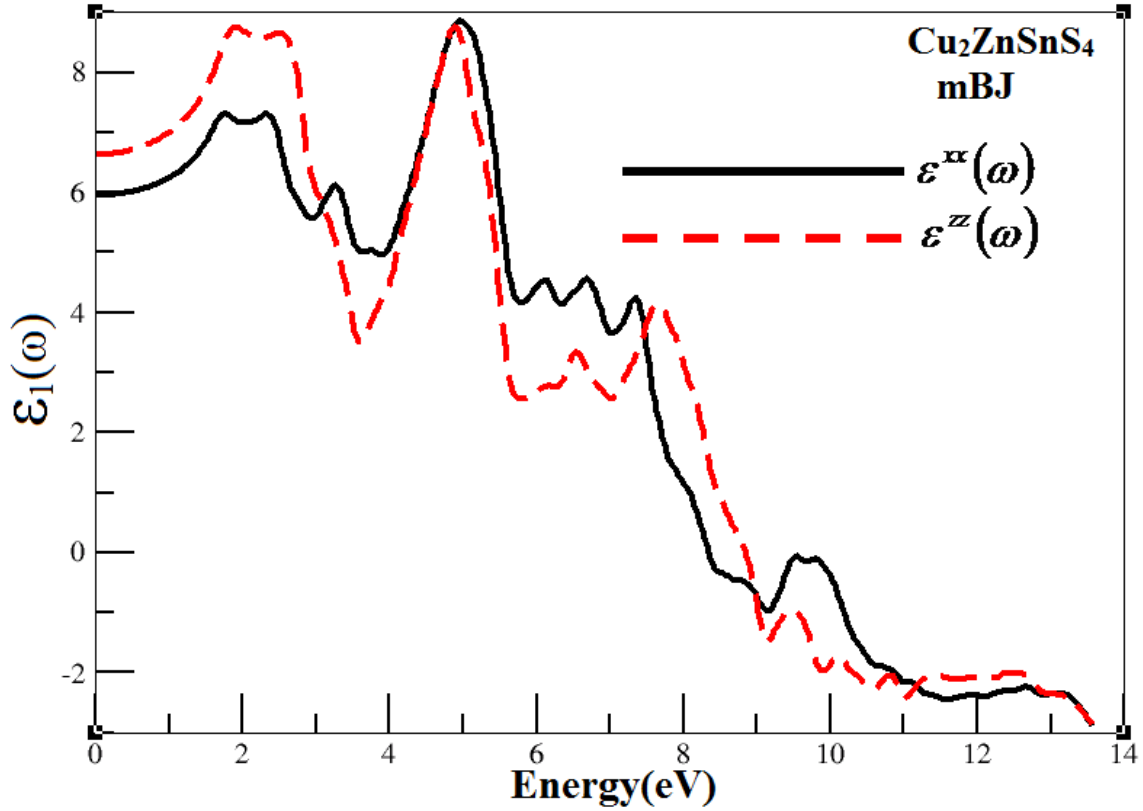
Cu2ZnSnS4
mBJ
$\varepsilon^{xx}(\omega)$
$\varepsilon^{zz}(\omega)$
$\varepsilon_1(\omega)$
Energy(eV)

(c)

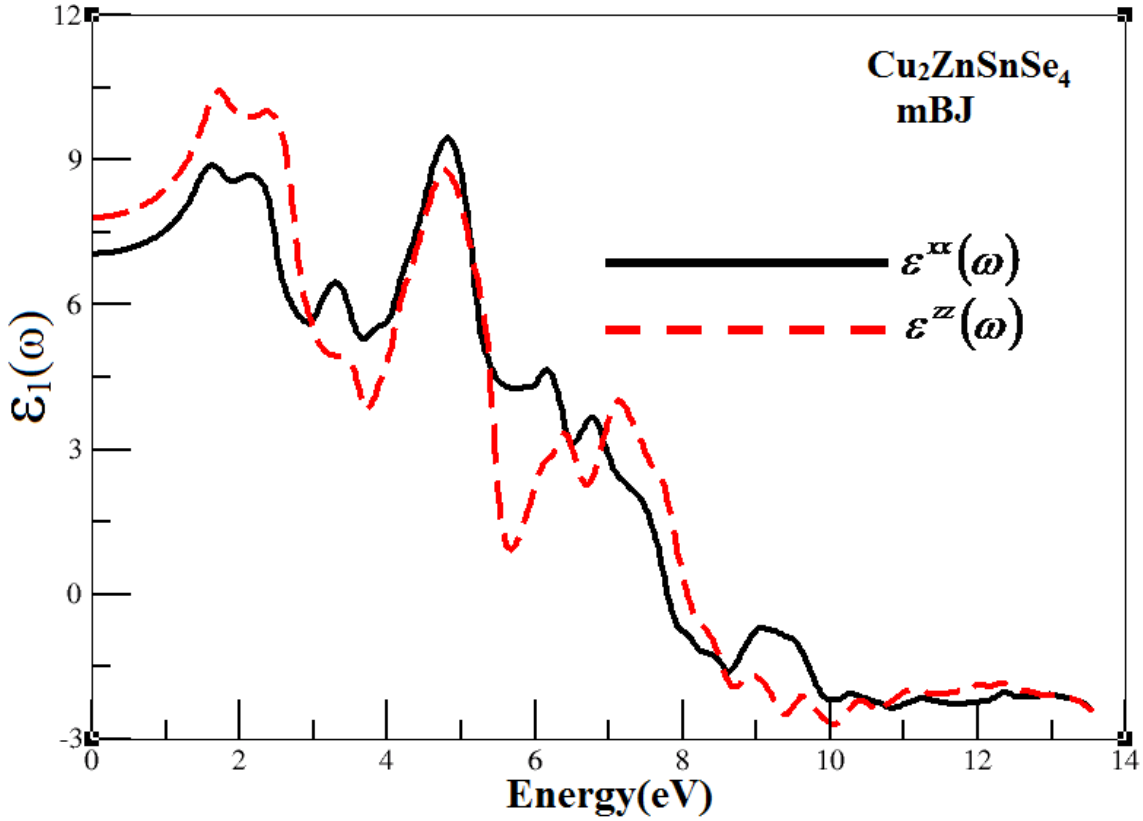
Cu2ZnSnSe4
mBJ
$\varepsilon^{xx}(\omega)$
$\varepsilon^{zz}(\omega)$
$\varepsilon_1(\omega)$
Energy(eV)

(d)

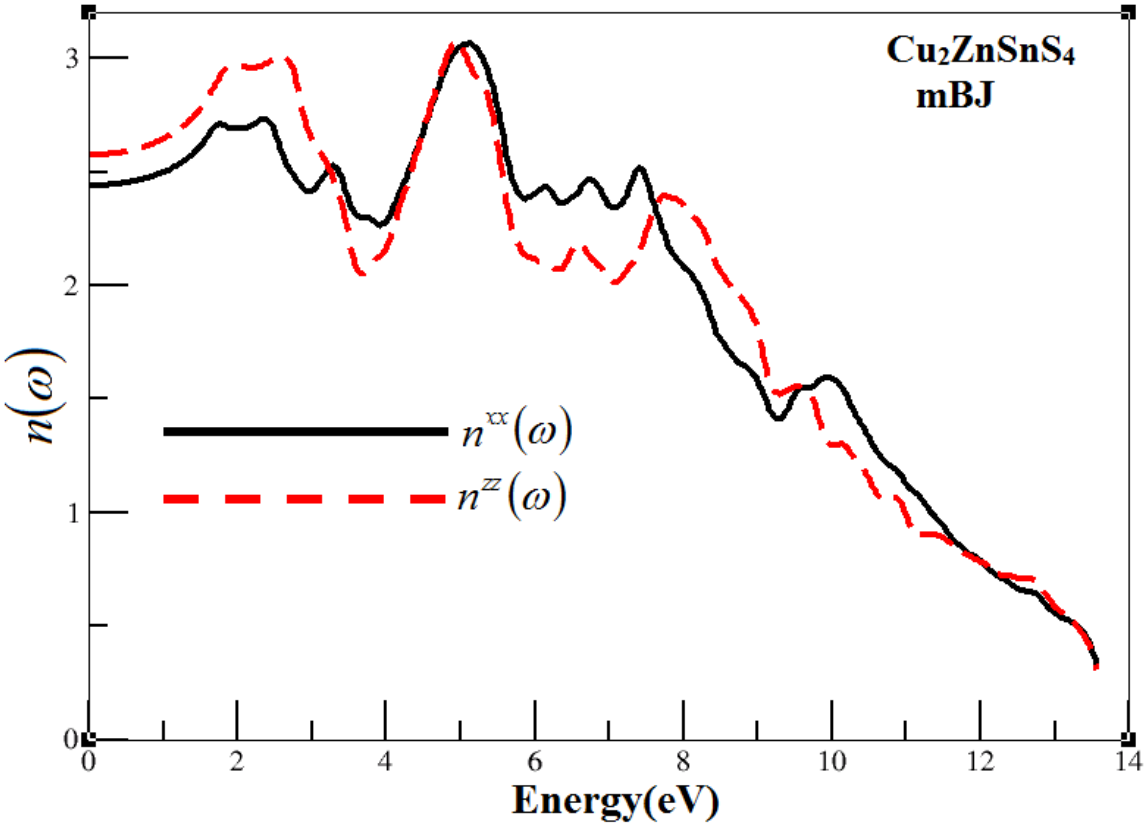
Cu2ZnSnS4
mBJ
n(ω)
$n^{xx}(\omega)$
$n^{zz}(\omega)$
0
1
2
3
0
2
4
6
8
10
12
14
Energy(eV)

(e)

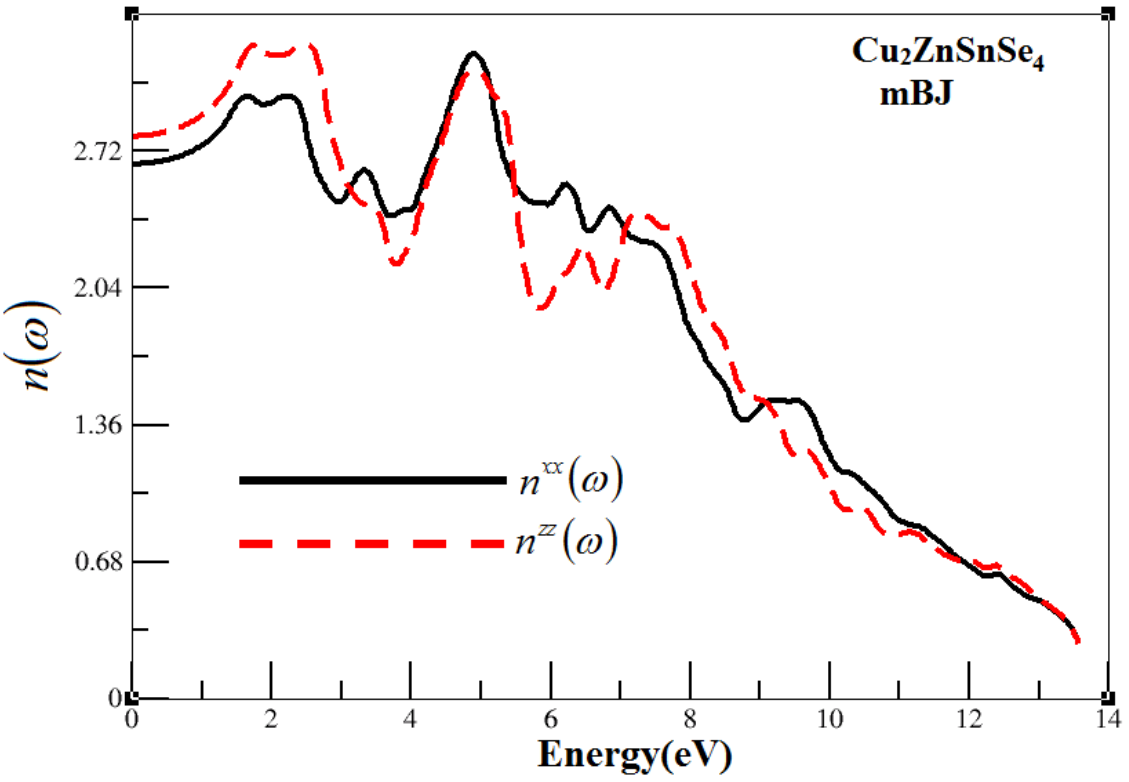
Cu2ZnSnSe4
mBJ
n(ω)
$n^{xx}(\omega)$
$n^{zz}(\omega)$
0
0.68
1.36
2.04
2.72
0
2
4
6
8
10
12
14
Energy(eV)

(f)

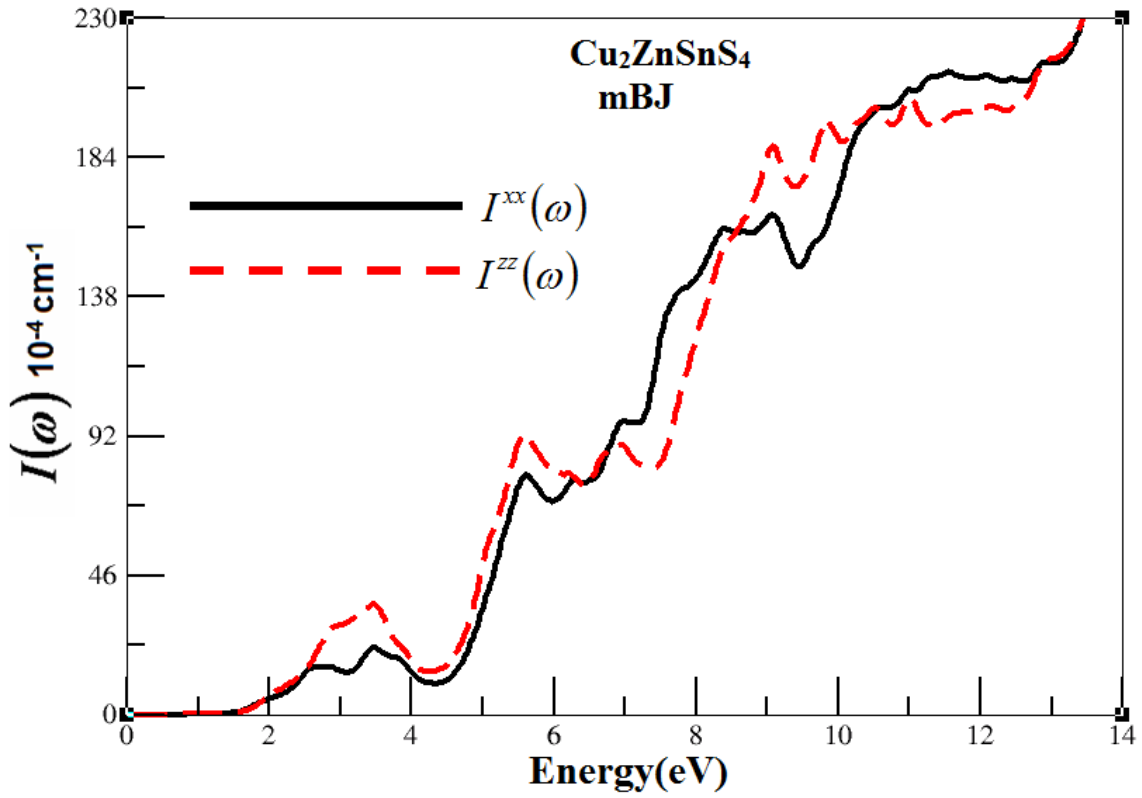
Cu2ZnSnS4
mBJ
$I^{xx}(\omega)$
$I^{zz}(\omega)$
$I(\omega)$ 10-4 cm-1
Energy(eV)
0
46
92
138
184
230
0
2
4
6
8
10
12
14

(g)

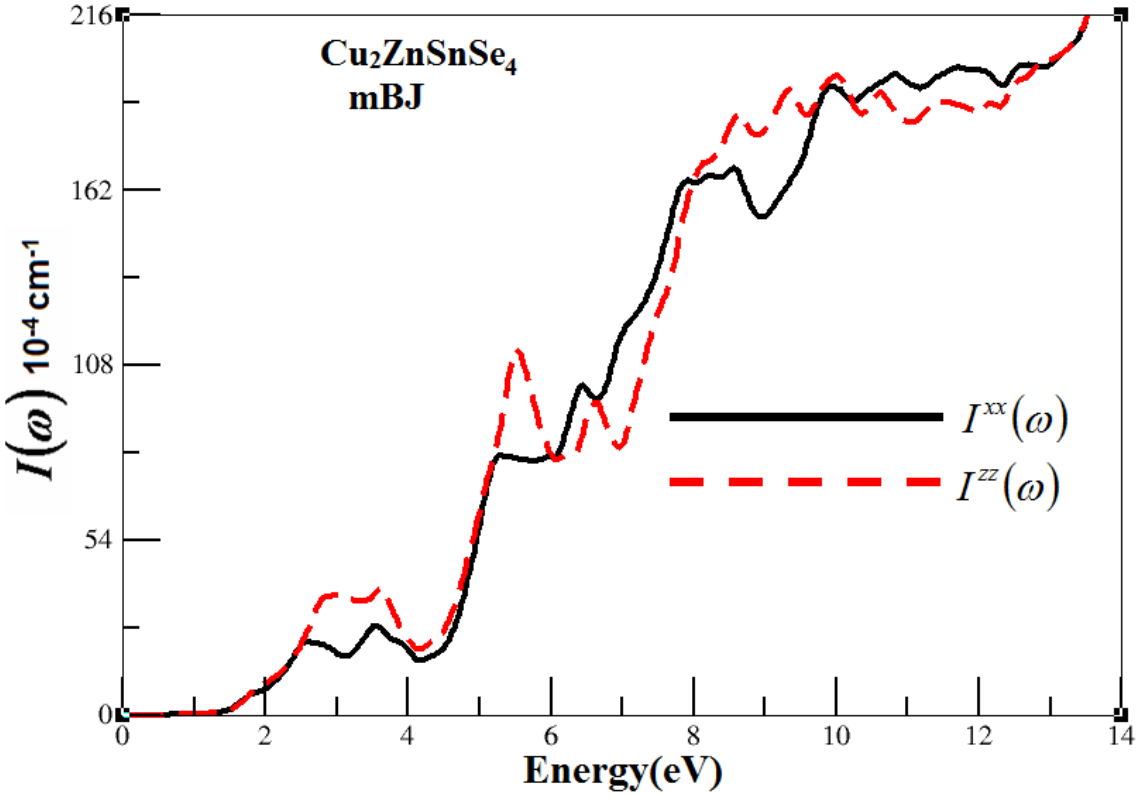
Cu2ZnSnSe4
mBJ
$I^{xx}(\omega)$
$I^{zz}(\omega)$
$I(\omega)$ 10-4 cm-1
Energy(eV)
0
54
108
162
216
0
2
4
6
8
10
12
14

(h)

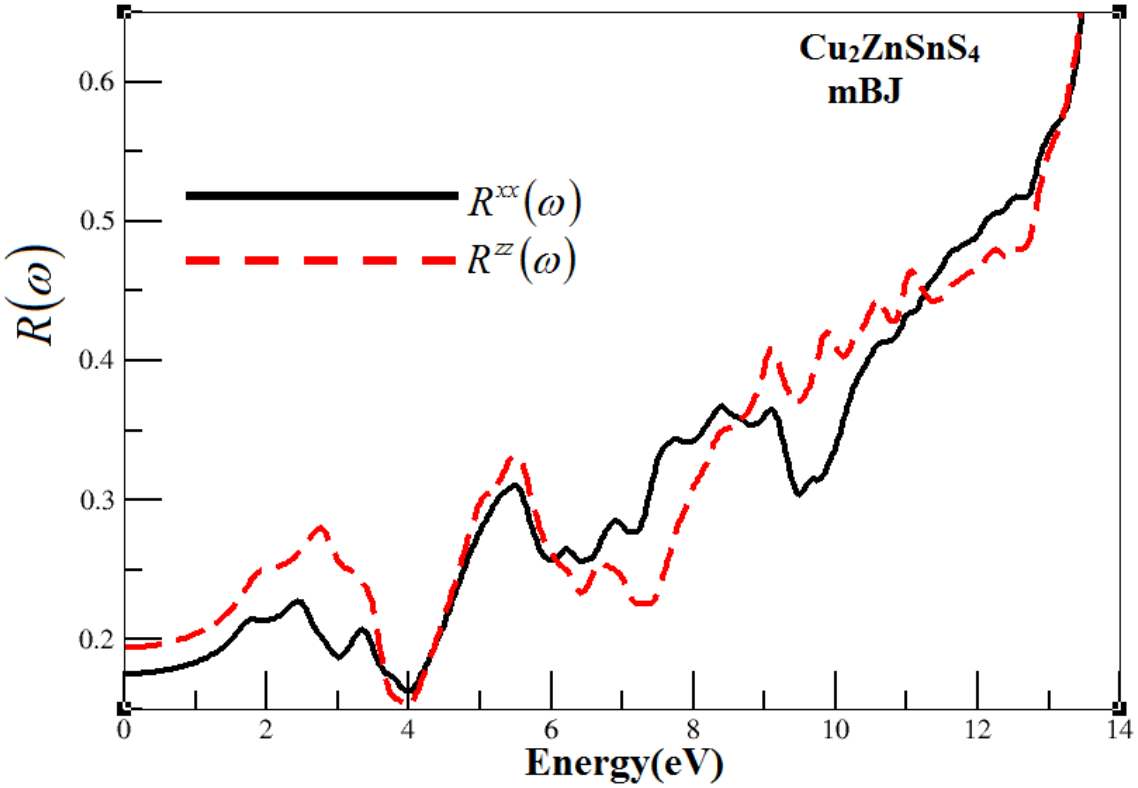
Cu2ZnSnS4
mBJ
$R^{xx}(\omega)$
$R^{zz}(\omega)$
$R(\omega)$
0.2
0.3
0.4
0.5
0.6
0
2
4
6
8
10
12
14
Energy(eV)

(i)

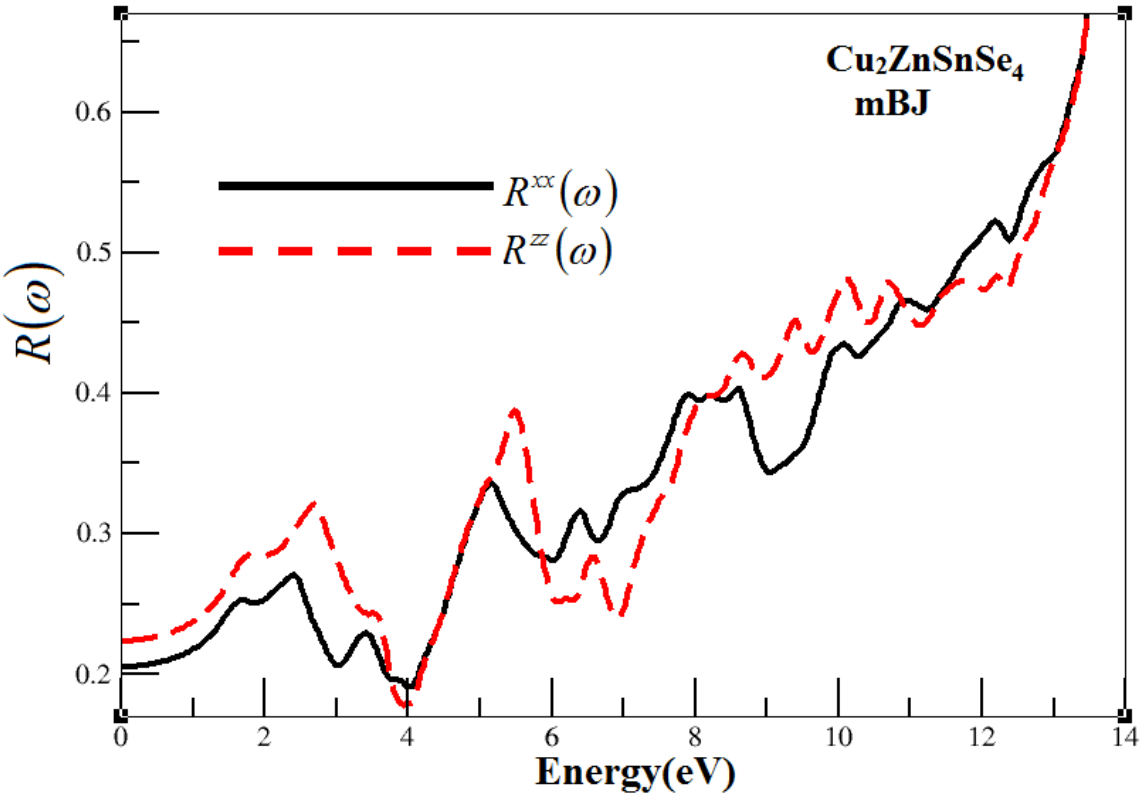
Cu2ZnSnSe4
mBJ
$R^{xx}(\omega)$
$R^{zz}(\omega)$
$R(\omega)$
0.2
0.3
0.4
0.5
0.6
0
2
4
6
8
10
12
14
Energy(eV)

(j)

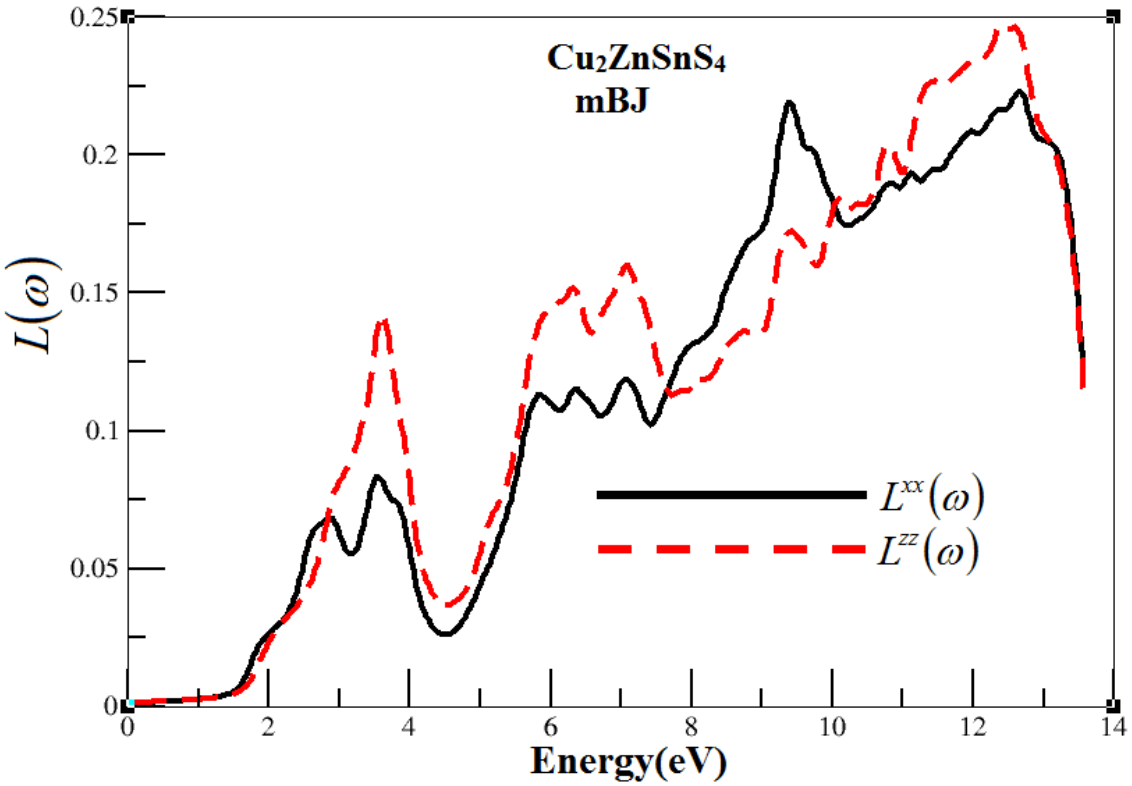

(k)

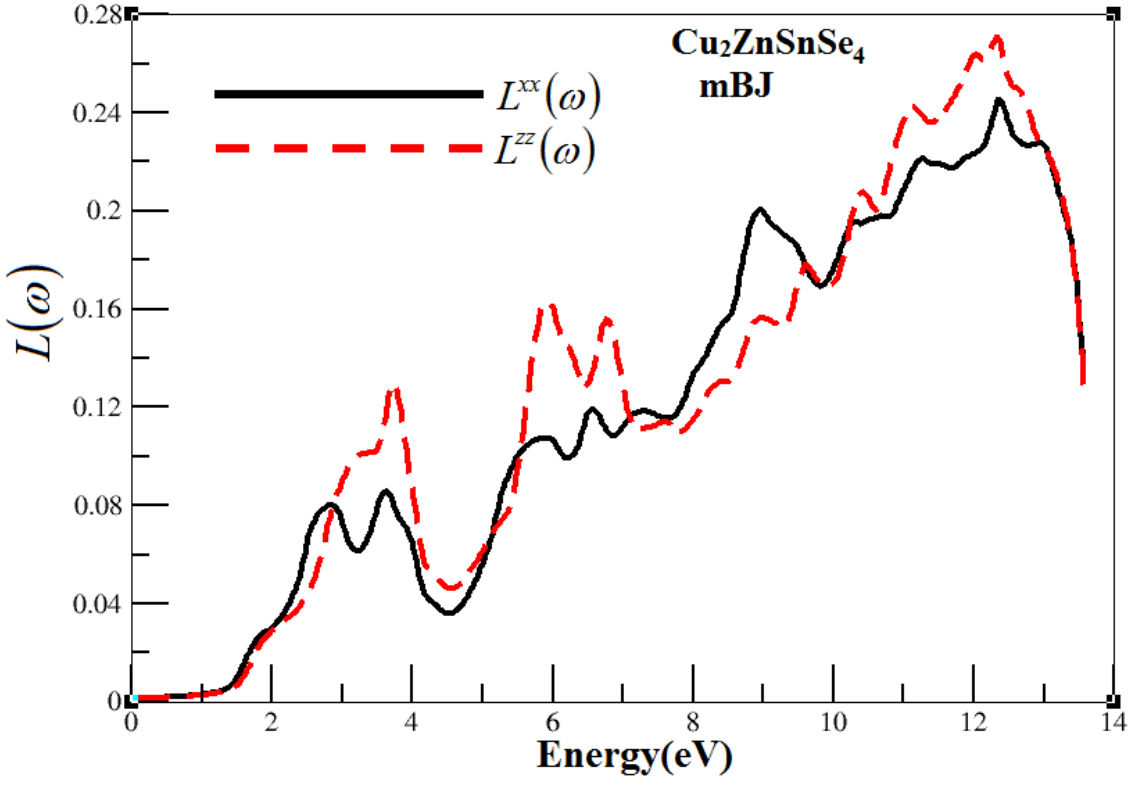

(l)

Figure 5. Calculated $\varepsilon_2^{xx}(\omega)$ (**dark solid curve-black color online**) and $\varepsilon_2^{zz}(\omega)$ (light dashed curve-red color online) dispersion spectra for different apporaches: mBJ with scissors correction for (a) Cu_2ZnSnS_4 and (b) $Cu_2ZnSnSe_4$; Calculated $\varepsilon_1^{xx}(\omega)$ (**dark solid curve-black color online**)

and $\varepsilon_1^{zz}(\omega)$ (light dashed curve-red color online) dispersion spectra: mBJ with scissors correction for (c) Cu_2ZnSnS_4 and (d) $Cu_2ZnSnSe_4$; Calculated $n^{xx}(\omega)$ (**dark solid curve-black color online**) and $n^{zz}(\omega)$ (light dashed curve-red color online) dispersion spectra: mBJ with scissors correction for (e) Cu_2ZnSnS_4 and (f) $Cu_2ZnSnSe_4$; Calculated $I^{xx}(\omega)$ (**dark solid curve-black color online**) and $I^{zz}(\omega)$ (light dashed curve-red color online) dispersion spectra: mBJ with scissors correction for (g) Cu_2ZnSnS_4 and (h) $Cu_2ZnSnSe_4$; Calculated $R^{xx}(\omega)$ (**dark solid curve-black color online**) and $R^{zz}(\omega)$ (light dashed curve-red color online) dispersion spectra: mBJ with scissors correction for (i) Cu_2ZnSnS_4 and (j) $Cu_2ZnSnSe_4$; Calculated $L^{xx}(\omega)$ (**dark solid curve-black color online**) and $L^{zz}(\omega)$ (light dashed curve-red color online) dispersion spectra: mBJ with scissors correction for (k) Cu_2ZnSnS_4 and (m) $Cu_2ZnSnSe_4$.

Fig. 5a and b, confirm that there exist a considerable anisotropy between $\varepsilon_2^{xx}(\omega)$ and $\varepsilon_2^{zz}(\omega)$ spectra. Possessing the dispersion of imaginary part of dielectric function the real part can be evaluated using Kramers-Kronig integral relations [37]. The calculated dispersions of real part of dielectric function $\varepsilon_1^{xx}(\omega)$ and $\varepsilon_1^{zz}(\omega)$ are shown in Fig. 5c and d. Again it show considerable anisotropy among $\varepsilon_1^{xx}(\omega)$ and $\varepsilon_1^{zz}(\omega)$ except at the low energy tail. The calculated optical dielectric constants at zero energy limit $\varepsilon_1^{xx}(0)$ and $\varepsilon_1^{zz}(0)$ are equal to 5.94, 6.61 and 7.04, 7.80, for Cu_2ZnSnS_4 and $Cu_2ZnSnSe_4$,respectively.

Fig.5 (e-l) shows the dispersion for non zero tensor components of refractive index $n(\omega)$, extinction coefficient $k(\omega)$, absorption coefficient $I(\omega)$, reflectivity spectra $R(\omega)$ and energy loss function $L(\omega)$. Complex refractive index ($\tilde{n}(\omega) = n(\omega) + ik(\omega)$) describes the refraction as well as well absorption of the compounds. It consists of two parts; the real part , $n(\omega)$, is just the refractive index second-order tensor while the other part, $k(\omega)$, is the extinction tensor which describes the loss of photon energy during propagation through the optical medium. As these compounds have tetragonal symmetry, only two tensor components (parallel and perpendicular to the **c**- axis with respect to the polarization of the optical field) are required to describe all the optical properties. The parallel and perpendicular components of refractive index ($n^{\parallel}$ and $n^{\perp}$, respectively) and extinction coefficient ($k^{\parallel}$ and $k^{\perp}$) define all the linear optical properties. The calculated non zero tensor components of static refractive index $n^{xx}(0)$ and $n^{zz}(0)$ are 2.42 and 2.56 for Cu_2ZnSnS_4 and 2.65, 2.79 for $Cu_2ZnSnSe_4$. Penn's model [38] claims that $\varepsilon_1(0)$ depends on band gap of the material and $\varepsilon_1(0)$ is directly related to the n (0) by the relation $n(\omega) = \sqrt{\varepsilon_1(0)}$. They are enhanced beyond the zero frequency limits reaching their maximum values. Beyond the maximum value they start to decrease and with few oscillations they go beyond unity. In this region (n<1) the phase velocity of the photons increases approaching to universal constant (C). However the group velocity always remains less than the C, as a consequence the relativity relations are not effected [39]. The spectra are shifted towards lower energy by changing the cations from S to Se. The variation is in accordance to the decreasing in the band gap. The calculated refractivity for Cu_2ZnSnS_4 and $Cu_2ZnSnSe_4$, are illustrated in Figs. 5 e and f.

The absorption spectra of Cu_2ZnSnS_4 and $Cu_2ZnSnSe_4$ (Figs. 5 g and h) show that these materials start absorbing the radiation at the wavelength below 775 nm and 861.1 nm, respectively. The absorption spectra show the highest value at 13.5 eV corresponding to the minimum value of $\varepsilon_1(\omega)$ and $\varepsilon_2(\omega)$ shown in Fig.5a-d.

Frequency dependent reflectivity $R^{zz}(\omega)$ and $R^{xx}(\omega)$ parallel and perpendicular spectra components to the electric field, are calculated and depicted in Figs. 5 i and j. The reflectivity spectra of the compounds start from the zero frequency which defines the static part of the reflectivity components $R^{zz}(0)$ and $R^{xx}(0)$. These values are equal to 0.17 and 0.18 for Cu_2ZnSnS_4 and 0.20, 0.22 for $Cu_2ZnSnSe_4$ single crystals. The reflectivity spectra of the compounds are spectrally red shifted during replacing anions of S by Se. The $L(\omega)$ described the energy loss of fast electron traveling in the material (Figs. 5 k and l). The sharp spectral peaks produced in $L(\omega)$ around 12.5 eV are due to the occurence of plasmon excitations [40].

4. CONCLUSION

The full potential linear augmented plane wave (FPLAPW) method in a scalar relativistic version, was applied for calculating the electronic structure of the two promising solar cell crystals Cu_2ZnSnS_4 and $Cu_2ZnSnSe_4$. The PDOS helps to identify the angular momentum character of the various structures, and to study the degree of the hybridization between states. We found that there exists weak/strong hybridization between the states. The optical spectra are shifted towards lower energy by changing the cations from S to Se. The variation is in accordance to the decreasing in the band gap. The absorption spectra of Cu_2ZnSnS_4 and $Cu_2ZnSnSe_4$ show that these materials start absorbing the radiation at the wavelength below 775 nm and 861.1 nm, respectively. The absorption spectra show the highest value at 13.5 eV corresponding to the minimum value of $\varepsilon_1(\omega)$ and $\varepsilon_2(\omega)$. It was found that the calculated optical dielectric constants at zero energy limit $\varepsilon_1^{xx}(0)$ and $\varepsilon_1^{zz}(0)$ are equal to 5.94, 6.61 and 7.04, 7.80, for Cu_2ZnSnS_4 and $Cu_2ZnSnSe_4$,respectively.

AKNOWLEDEGMENT
The result was developed within the CENTEM project, reg. no. CZ.1.05/2.1.00/03.0088, co-funded by the ERDF as part of the Ministry of Education, Youth and Sports OP RDI programme. School of Material Engineering, Malaysia University of Perlis, Malaysia.

References

1. S. Siebentritt, S. Schorr, Prog. *Photovoltaics Res. Appl.* 20 (2012) 512.
2. D.B. Mitzi, O. Gunawan, T.K. Todorov, K. Wang, S. Guha, *Sol. Energy Mater. Sol. Cells* 95 (2011) 1421.
3. S. Ahmed, K.B. Reuter, O.Gunawan, L. Guo, L.T. Romankiw,H. Deligianni, *Adv. Energy Mater*. 2 (2012) 253
4. D. Aaron, R. Barkhouse, O. Gunawan, T. Gokmen, T.K. Todorov, D.B. Mitzi, Prog. *Photovoltaics Res. Appl.* 20 (2012) 6.

5. B. Shin, O. Gunawan, Y. Zhu, N.A. Bojarczuk, S.J. Chey, S. Guha, Prog. *Photovoltaics Res. Appl.* Vol 21, (2013) pp. 72-76
6. S.R. Hall, J.T. Syzmanski, J.M. Stewart, Can. *Miner.* 16 (1978) 131.
7. S. Schorr, *Thin Solid Films* 515 (2007) 5985.
8. S. Schorr, H.J. Hoebler, M. Tovar, *Eur. J. Mineral*. 19 (2007) 65.
9. J. Paier, R. Asahi, A. Nagoya, G. Kresse, *Phys. Rev. B* 79 (2009) 115126.
10. K. Todorov, K. B. Reuter, and D. B. Mitzi, *Adv. Mater. Weinheim, Ger*. 22, (2010) E156
11. A. Redinger, D. M. Berg, P. J. Dale, and S. Siebentritt, *J. Am. Chem. Soc*. 133, (2011) 3320
12. C. Persson, *J. Appl. Phys.* 107, (2010) 053710
13. S. Chen, X. G. Gong, A. Walsh, and S.-H. Wei, *Appl. Phys. Lett*. 94, (2009) 041903
14. S. Chen, A. Walsh, Y. Luo, J.-H. Yang, X. G. Gong, and S.-H. Wei, *Phys. Rev. B* 82, (2010) 195203
15. J. Paier, R. Asahi, R. Wahl, and G. Kresse, *Phys. Rev. B* 79, 115126 (2009).
16. S. Chen, X. G. Gong, A. Walsh, and S.-H. Wei, *Appl. Phys. Lett*. 96, (2010) 021902; S. Chen, J.-H. Yang, X. G. Gong, A. Walsh, and S.-H. Wei, *Phys. Rev. B.* 81, (2010) 245204.
17. A. Nagoya, R. Asahi, R. Wahl, and G. Kresse, *Phys. Rev. B*. 81, (2010) 113202
18. Hiroshi Nozaki, Tatsuo Fukano, Shingo Ohta, Yoshiki Seno, Hironori Katagirib, Kazuo Jimbo. 524, (2012) 22–25
19. Xiancong He, Honglie Shen. j. *Physica B: Condensed Matter*. 406, (2011) 4604–4607
20. Clas Persson. J. Appl. Phys. 107, (2010) 053710
21. Shiyou Chen, X. G. Gong, Aron Walsh, Su-Huai Wei. *APPLIED PHYSICS LETTERS.* 94, (2009) 041903
22. Bonazzi P., Bindi L., Bernardini G.P., Menchetti S. *Canadian Mineralogist.* 41, (2003), p. 639-647.
23. Olekseyuk I.D., Gulay L.D., Dydchak I.V., Piskach L.V., Parasyuk O.V., Marchuk O.V. *J. Alloys. Compd.* 340 (2002), p. 141 - 145.
24. A.O. Fedorchuk, O.V. Parasyuk, I.V. Kityk. *Maer.ChemPhys*. V.139, (2013), 92
25. Emsley J. The Elements (Oxford University Press, Oxford, 1997).
26. P. Blaha, K. Schwarz, G. K. H. Madsen, D. Kvasnicka and J. Luitz, WIEN2k, Vienna University of Technology, Austria (2001).
27. W. Kohn and L. J. Sham, *Phys. Rev*. A 140, 1133 (1965).
28. J. P. Perdew, S. Burke, and M. Ernzerhof, *Phys. Rev. Lett*. 77 (1996) 3865.
29. E. Engel, S. H. Vosko, *Phys. Rev. B.* 47 (1993) 13164.
30. Fabien Tran and Peter Blaha *Phys. Rev. Lett*. 102, (2009) 226401
31. Shiwu Gao, *Computer Physics Communications*, 153, (2003) 190
32. Karlheinz Schwarz, *Journal of Solid State Chemistry*. 176, (2003) 319
33. Dovgii, *Ukr.Phys.Journal*, 1984
34. A. Delin, P. Ravindran, O. Eriksson, J. M. Wills, Int. J.Quant. Chem. 69 (1998) 349-
35. 358.
36. Ya.O.Dovgii, .I.V. Kityk, M.I. Kolinko, A.S. Krochuk, A.V. Franiv & M.K. Zamorskii. *Phys.Stat.Sol.* V.167B. (1991).P.637-646.
37. K.Nouneh, A.H.Reshak, S.Auluck, I.V.Kityk, R.Viennois, S.Benet, S.Charar. *Journal of Alloys and Compounds*, V.437, (2007), pp.39-46; Ali Hussain Reshak, Dalibor Stys, S. Auluck and I. V. Kityk. . *Journal Physical Chemistry B*. V. 113, (2009), pp 12648–12654.
38. H. Tributsch, A. *Naturforsch.* 32A (1977) 972.
39. D.R. Penn, Phys. Rev. B.128 (1962) 2093-2097.
40. M. Fox, Optical Properties of Solids, Oxford University Press, 2001.
41. L. Marton, *Rev. Mod. Phys*. 28 (1956) 172-184.
42. A. H. Reshak, H. Kamarudin, I. V. Kityk, S.Auluck. *journal of material science*, 48 (2013) 5157-5162

43. Sikander Azam, A. H. Reshak. *Int. J. Electrochem. Sci*., 8 (2013) 10359 – 10375.
44. A.H. Reshak, S.A. Khan. *Computational Materials Science* 78 (2013) 91–97.
45. Saleem Ayaz Khan, A. H. Reshak. *Int. J. Electrochem. Sci*., 8 (2013) 9459 – 9473.
46. Ali H. Reshak, S. Auluck, I.V. Kityk. *Current Opinion in Solid State and Materials Science* 12 (2008) 14–18.

© 2014 by ESG (www.electrochemsci.org)